AD-A120 428 ELECTROOPTICAL DEVICES(U) MASSACHUSETTS INST OF TECH LEXINGTON LINCOLN LAB C E HURWITZ 30 SEP 81 ESD-TR-81-380 F19628-80-C-0002 1/1

UNCLASSIFIED F/G 20/5 NL

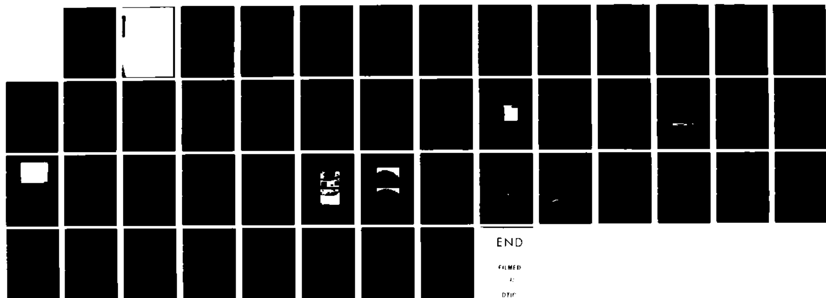

END

FILMED

DTIC

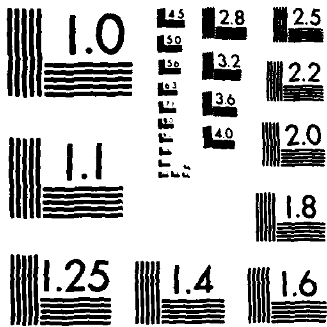

MICROCOPY RESOLUTION TEST CHART
NATIONAL BUREAU OF STANDARDS-1963-A

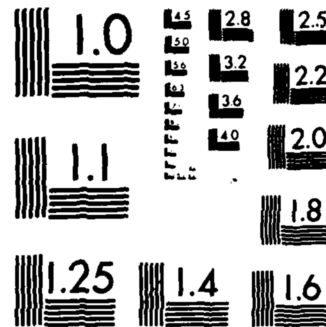

MICROCOPY RESOLUTION TEST CHART
NATIONAL BUREAU OF STANDARDS-1963-A

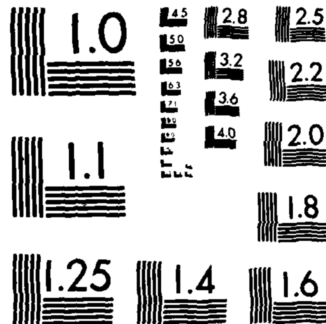

MICROCOPY RESOLUTION TEST CHART
NATIONAL BUREAU OF STANDARDS-1963-A

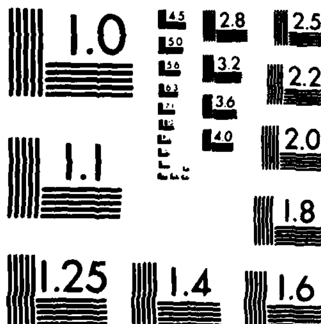

MICROCOPY RESOLUTION TEST CHART
NATIONAL BUREAU OF STANDARDS-1963-A

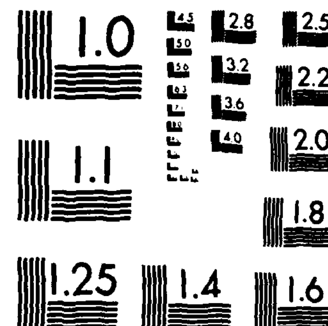

MICROCOPY RESOLUTION TEST CHART
NATIONAL BUREAU OF STANDARDS-1963-A

AD A120428

The work reported in this document was performed at Lincoln Laboratory, a center for research operated by Massachusetts Institute of Technology, with the support of the Rome Air Development Center under Air Force Contract F19628-80-C-0002.

This report may be reproduced to satisfy needs of U.S. Government agencies.

The views and conclusions contained in this document are those of the contractor and should not be interpreted as necessarily representing the official policies, either expressed or implied, of the United States Government.

The Public Affairs Office has reviewed this report, and it is releasable to the National Technical Information Service, where it will be available to the general public, including foreign nationals.

This technical report has been reviewed and is approved for publication.

FOR THE COMMANDER

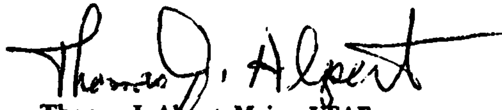

Thomas J. Alpert, Major, USAF
Chief, ESD Lincoln Laboratory Project Office

Non-Lincoln Recipients

PLEASE DO NOT RETURN

Permission is given to destroy this document when it is no longer needed.

MASSACHUSETTS INSTITUTE OF TECHNOLOGY
LINCOLN LABORATORY

ELECTROOPTICAL DEVICES

SEMIANNUAL TECHNICAL SUMMARY REPORT
TO THE
ROME AIR DEVELOPMENT CENTER

1 APRIL — 30 SEPTEMBER 1981

ISSUED 20 AUGUST 1982

Approved for public release; distribution unlimited.

LEXINGTON MASSACHUSETTS

ABSTRACT

This report covers work carried out with the support of the Rome Air Development Center during the period 1 April through 30 September 1981.

GaInAsP/InP lasers with highly uniform and reproducible threshold characteristics have been fabricated by careful control of layer thickness and morphology. Reduced threshold current densities of 4 to 5 kA/cm^2-µm were routinely achieved for a wide range of active layer thicknesses.

Broad-area Be-implanted GaInAsP/InP laser diodes have been fabricated. The best results have been obtained using Be implanted and annealed under conditions which minimize diffusion of the implanted ions. Reduced threshold current densities averaging 6 to 7 kA/cm^2-µm and as low as 4.2 kA/cm^2-µm have been measured and are comparable with those of conventional laser structures. Precise control over the thickness and doping of the InP cap layer is required to achieve reproducible results.

GaInAsP/InP diode lasers have been fabricated with an intracavity electroabsorption modulator. The additional loss produced by operating the modulator near maximum reverse bias increased the laser threshold by a factor of as much as 2.9 relative to the threshold with the modulator open-circuited. Large depth of modulation of the laser output has been achieved at frequencies up to 2.5 GHz, the system measurement limit.

A technique has been developed to monolithically integrate a passive waveguide with a GaInAsP/InP double-heterostructure laser for potential use in fabricating modulators and integrated external cavities. Initial tests of broad-area lasers with 350-µm passive waveguide sections showed threshold current densities of 2.4 to 3.1 kA/cm^2.

The noise properties of InP avalanche photodiodes (APDs) with the n^+-n-p^+ inverted-mesa structure have been characterized. The detectors were found to have essentially the same noise behavior as the GaInAsP/InP 1.3-µm APDs with InP p-n junctions, i.e., an excess noise factor which is very low ($F \approx 3$ at $M = 10$) up to gains of 10 to 20 and which rises rapidly for larger multiplication. The results indicate that the noise characteristics of the GaInAsP/InP devices are determined primarily by those of the InP p-n junctions.

Hole diffusion lengths in n-InP of 12 μm have been determined by measuring the increase in collection efficiency of an InP avalanche photodiode as a function of reverse bias. This diffusion length is nearly an order of magnitude greater than the previously reported values measured by surface photovoltage and electron-beam-induced (EBIC) techniques.

Accession For
NTIS GRA&I ☒
DTIC TAB ☐
Unannounced ☐
Justification
By
Distribution/
Availability Codes
Dist | Avail and/or Special
A

TABLE OF CONTENTS

	Abstract	iii
I.	THRESHOLD CHARACTERISTICS OF GaInAsP/InP DOUBLE-HETEROSTRUCTURE LASERS	1
II.	Be-IMPLANTED GaInAsP/InP DOUBLE-HETEROSTRUCTURE DIODE LASERS	5
III.	INTRACAVITY LOSS MODULATION OF GaInAsP DIODE LASERS	19
IV.	MONOLITHIC INTEGRATION OF GaInAsP/InP LASERS WITH PASSIVE OPTICAL WAVEGUIDES	25
V.	NOISE CHARACTERISTICS OF InP AVALANCHE PHOTODIODES	31
VI.	DIFFUSION LENGTH OF HOLES IN n-InP	37
References		41

ELECTROOPTICAL DEVICES

I. THRESHOLD CHARACTERISTICS OF GaInAsP/InP DOUBLE-HETEROSTRUCTURE LASERS

There have been a number of investigations[1-5] of the threshold current densities of GaInAsP/InP double-heterostructure (DH) lasers with emission wavelengths around 1.3 μm. However, the reported data were generally scattered over a wide range, making the physical interpretation uncertain. In this work we have attempted a systematic study of 1.3-μm GaInAsP/InP lasers with special attention directed toward uniformity within a wafer and accuracy in the measurement of active layer thickness.

The double-heterostructure laser wafers were grown by conventional liquid-phase epitaxial growth techniques on Sn-doped ($n \cong 1 \times 10^{18}$ cm^{-3}) (100)-InP substrates. Some experiments on growth temperature and time were carried out to assure uniform thickness and good surface morphology in the InP buffer and cap layers. Broad-area lasers ~200 μm in width and ~500 μm in length were fabricated. Plated and alloyed Au/Zn/Au and Au/Sn/Au contacts were made to the p-type InP cap layer and n-type InP substrates, respectively, and the devices were separated by cleaving and saw-cutting. In addition to the room-temperature pulsed threshold current density, J_{th}, the active layer thickness d was also measured for each individual laser diode by using a scanning electron microscope. To improve the measurement for devices with $d < 2000$ Å, the mirror facets were etched in an aqueous solution of $K_3Fe(CN)_6$ and KOH in order to bring out the contrast between the $Ga_{0.27}In_{0.73}As_{0.63}P_{0.37}$ active layer and InP. The etching time was minimized to assure a negligible enhancement of the active layer thickness.[6]

The devices fabricated from each wafer showed good uniformity in J_{th}; only $\lesssim$10 percent of the tested devices did not lase or had abnormally high J_{th}. Figure I-1 shows the plot of J_{th} vs d for laser diodes fabricated from seven different wafers. The diode lengths L were typically between 440 and 550 μm. A "normalization" of each J_{th} to L = 500 μm was carried out by using the averaged slope in the J_{th} vs 1/L plot. The deviations of the

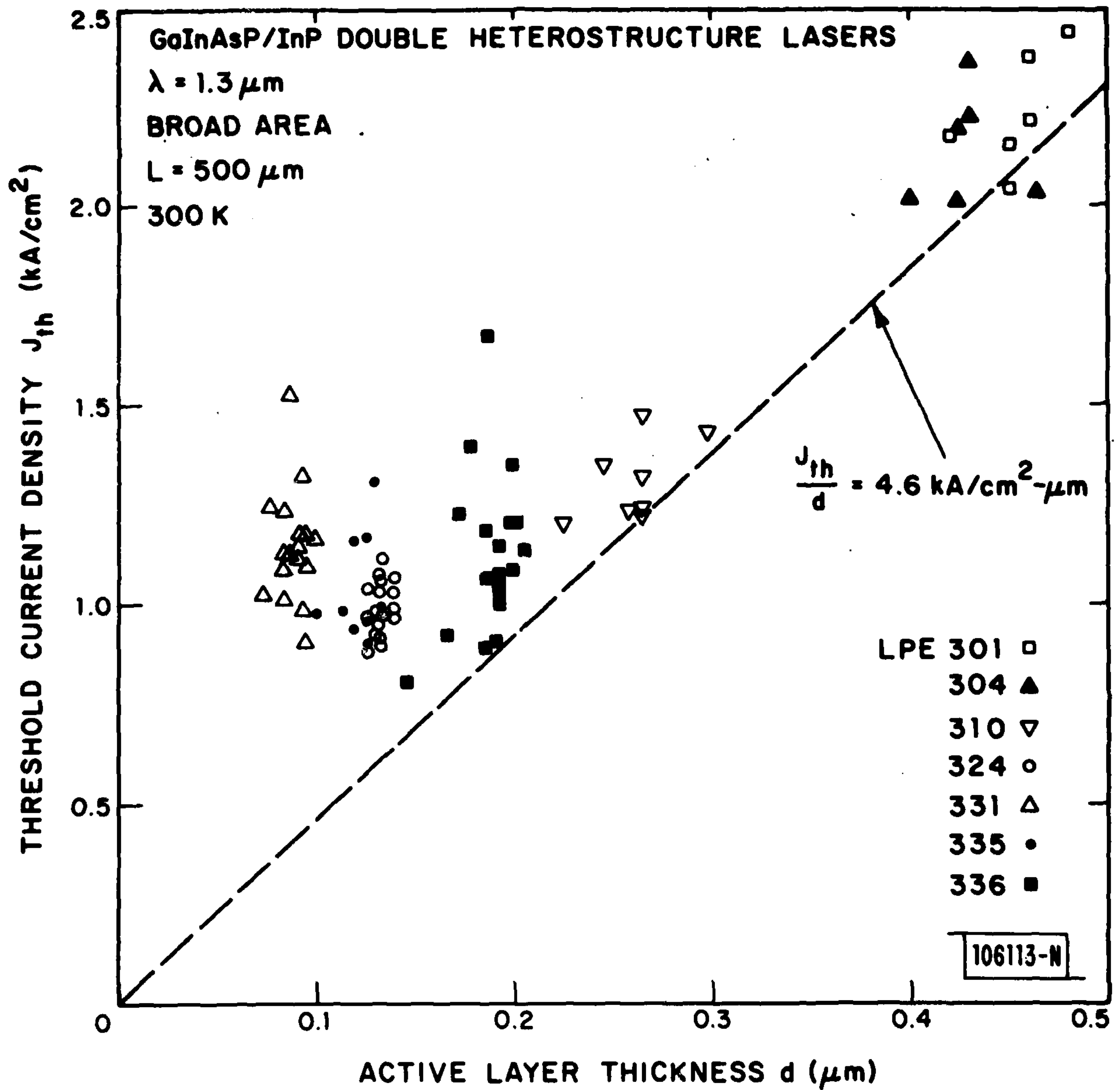

Fig. I-1. Plot of threshold current density vs active layer thickness for GaInAsP/InP double-heterostructure lasers fabricated from seven different wafers.

normalization factors from unity were less than 0.04. The wafer with best uniformity was LPE 324, in which only one device did not lase out of 30 tested. Moreover, 25 of the devices had J_{th}'s within ±10 percent of their average value. This wafer also had a very uniform active layer thickness as shown in Fig. I-1.

Figure I-2 shows the normalized threshold current density, J_{th}/d, plotted vs d for lasers of thicker active layers. In Fig. I-2, J_{th}/d decreases approximately 10 percent when d increases from 0.45 to 1.1 μm. This could be due to more reabsorption of spontaneous photons by thicker active layers.[7-9]

The low J_{th}'s obtained in this work are comparable to those of Itaya et al.[2] and Greene and Henshall[3] and are close to the lowest (0.67 kA/cm^2) reported by Nelson.[4] The wafer uniformity achieved in this work appears to be better than previously reported.[1-5]

Z.L. Liau
J.N. Walpole
G.W. Iseler

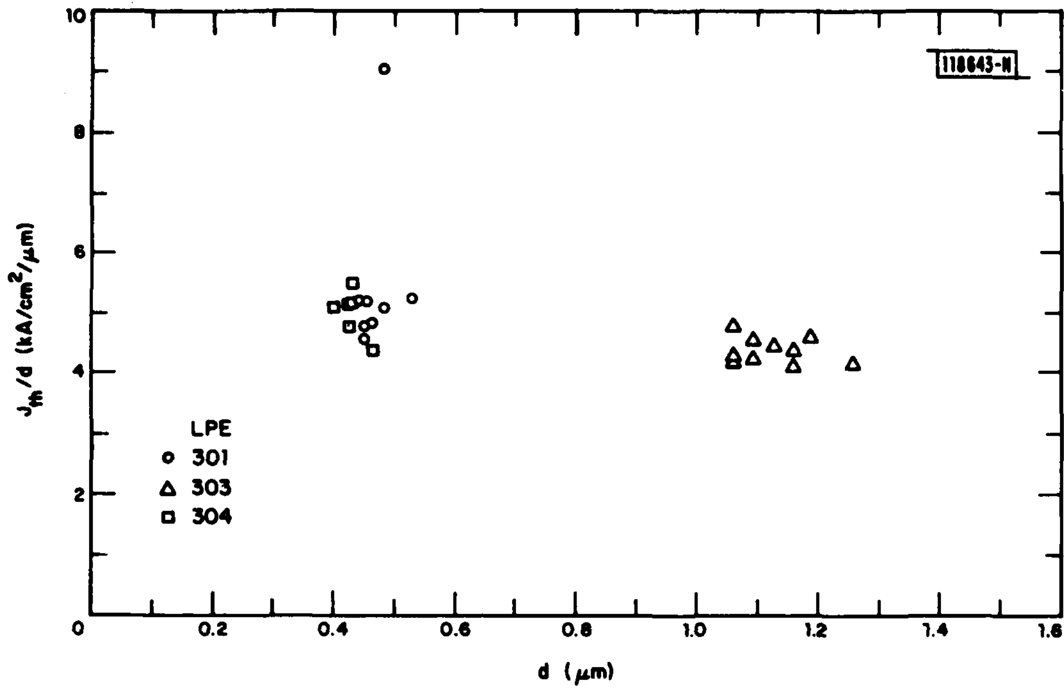

Fig. I-2. Plot of normalized threshold current density, J_{th}/d, vs active layer thickness, d, for GaInAsP/InP double-heterostructure lasers with d > 0.4 μm.

II. Be-IMPLANTED GaInAsP/InP DOUBLE-HETEROSTRUCTURE DIODE LASERS

Beryllium ion implantation followed by a diffusion of the implanted Be has been used to fabricate lasers in the GaAs/AlGaAs material system.[10,11] In this section, we report use of Be implantation to fabricate broad-area GaInAsP/InP double-heterostructure laser diodes operating at 1.3 μm. These lasers had threshold current densities comparable to those obtained using conventional Zn doping during the epitaxial growth of the InP cap layer. The use of implantation to selectively dope different areas of a heterostructure sample should provide significant advantages in the fabrication of more advanced laser structures[12] and the integration of laser diodes with other optical and microwave devices.[13]

The samples used in these experiments were standard GaInAsP/InP double-heterojunction wafers grown by liquid-phase epitaxy (LPE). Starting with an n^+-InP substrate, a tin-doped InP buffer layer with a carrier concentration of about 2×10^{18} cm^{-3} was grown first. This was followed by a GaInAsP active layer and an InP cap layer, both of which were n-type with a carrier concentration of (1 to 2) $\times 10^{17}$ cm^{-3}. As is discussed later, uniformity of both the thickness and the carrier concentration of the InP cap over the entire wafer is extremely important for the reproducible fabrication of Be-implanted lasers.

Although the results are not as well documented as in GaAs (Refs. 14-16), it has been reported that implanted Be in InP also has a concentration-dependent diffusion coefficient.[17,18] If the Be concentration is kept below (2 to 3) $\times 10^{18}$ cm^{-3}, the resulting p-n junctions are at a depth expected from LSS range theory*[19,20] (at least in material with a background n-type concentration greater than 10^{16} cm^{-3}). For high Be concentrations, the junctions are appreciably deeper than expected, with the depth increasing with implant dose and implant temperature.[17] The diffused Be profiles in InP (Ref. 18), however, do not appear to be as abrupt as in GaAs (Ref. 16).

---

*Only the projected range and projected standard deviation were used to determine the appropriate as-implanted profiles.

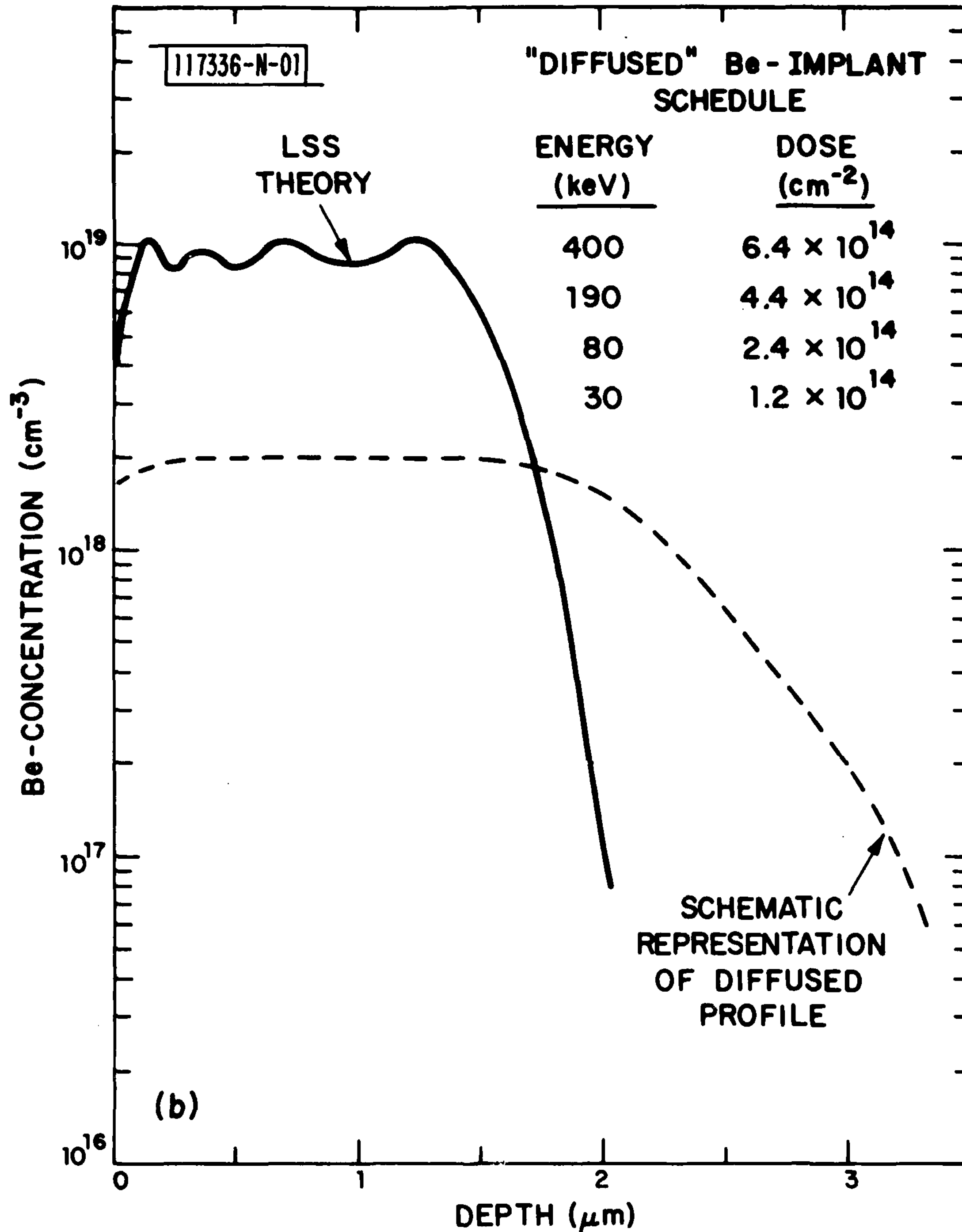

Fig. II-1. The predicted Be-implanted profiles of the two different types of implants used in these experiments: (a) implant schedule that results in minimal diffusion and (b) that which results in significant diffusion of the implanted Be.

This is substantiated by the capacitance-voltage measurements discussed later in this section.

To investigate the effects of this concentration-dependent diffusion on laser performance, two basically different Be-implant schedules were used in these experiments, one that results in minimal diffusion of the implanted Be and one that results in junctions ≈1.0 μm deeper than expected from LSS range theory.*[19,20]

The Be-implantation schedule used which results in minimal diffusion was 5.0×10^{13} cm^{-2} at 400 keV, 3.5×10^{13} cm^{-2} at 200 keV, 8.0×10^{13} cm^{-2} at 80 keV, and 3.0×10^{13} cm^{-2} at 30 keV. The profile predicted from LSS range theory using this schedule is shown in Fig. II-1(a). This hi-lo profile was chosen to provide the highest Be concentration near the surface consistent with minimal diffusion, but a lower concentration near the active layer to minimize free carrier absorption. Electrical activation of the implanted Be is expected[17] to be >50 percent for this implant schedule, with a higher percentage likely in the tail region. For the p-n junction to be at the InP-GaInAsP interface or in the quaternary, the InP cap should be ≈1.5 to 1.7 μm thick for a background carrier concentration of (1 to 2) x 10^{17} cm^{-3}. Caps that were grown too thick have been successfully etched to the desired thickness prior to implantation. Implantations using this "nondiffused" Be schedule were carried out with the GaInAsP/InP samples at either room temperature or 150°C.

For "diffused" Be-implanted lasers, a Be-implantation schedule which results in a flat LSS profile of 1×10^{19} cm^{-3} and a LSS junction depth about 1.0 μm less than the InP cap thickness was used. For example, Fig. II-1(b) shows the LSS profile for a Be-implant schedule of 6.4×10^{14} cm^{-2} at 400 keV, 4.4×10^{14} cm^{-2} at 190 keV, 2.4×10^{14} cm^{-2} at 80 keV, and 1.2×10^{14} cm^{-2} at 30 keV, which was used to fabricate "diffused" lasers on a wafer with a 3.0-μm-thick cap layer. For these high-concentration implants, the Be diffuses sufficiently during the post-implantation anneal to result in p-n

*Only the projected range and projected standard deviation were used to determine the appropriate as-implanted profiles.

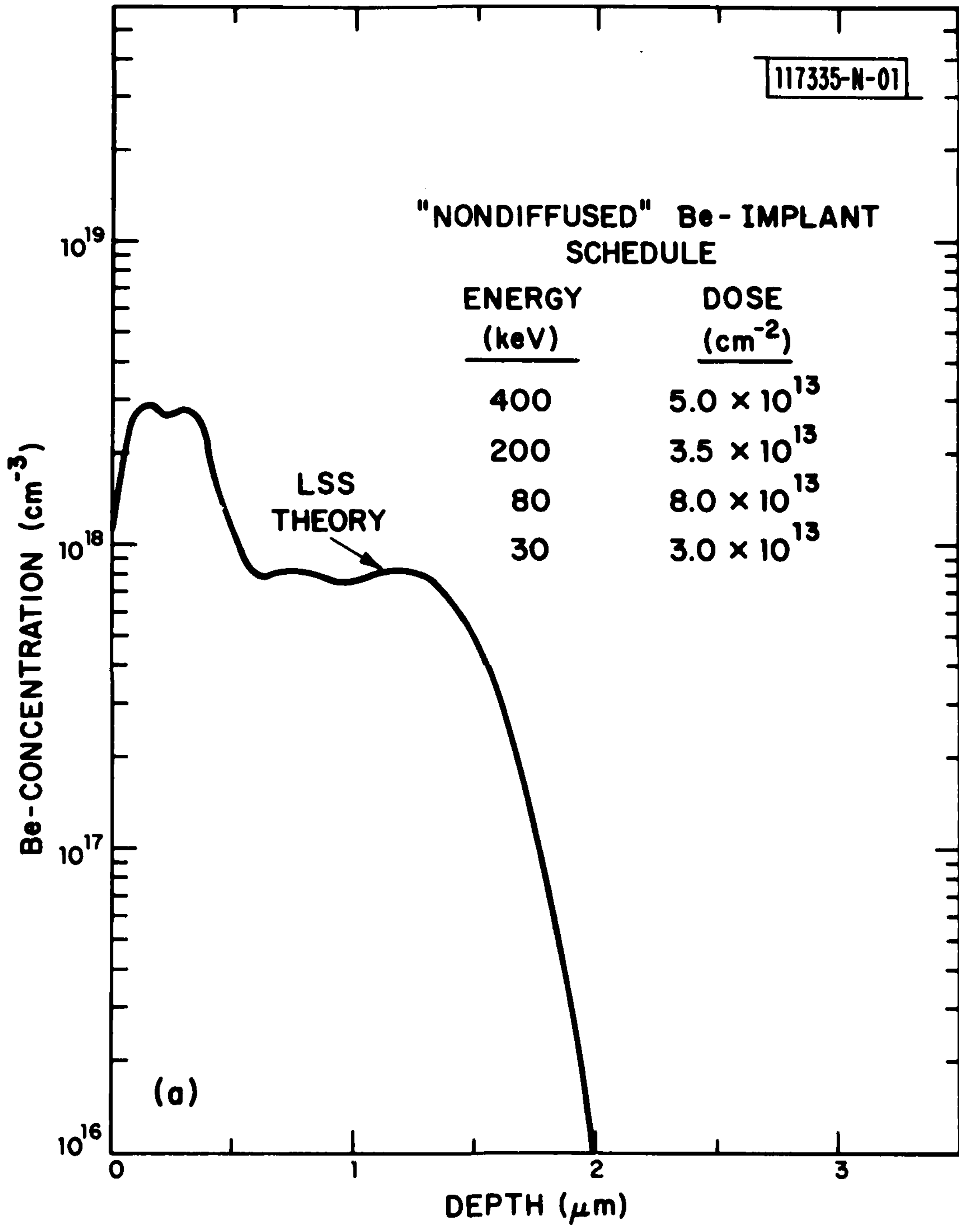

Fig. II-1. Continued.

junctions at the heterojunction interface or slightly into the GaInAsP layer. Samples were held at 150°C during implantation with a "diffused" implant schedule.

After implantation, all the samples were annealed at 750°C for 10 min. using a phosphosilicate glass (PSG) encapsulation plus a PH_3 overpressure.[17,21] Contact was made to the Be-implanted layer using a microalloyed plated Au/Zn/Au contact, while plated Au/Sn was used to contact the back of the n^+-InP substrate. Broad-area laser diodes approximately 200 x 500 μm in size with sawed sides and cleaved end faces were then made from each wafer. The cap and active layer thicknesses of selected areas of each wafer were determined using both optical and scanning-electron-beam (SEM) microscopy. Electron-beam-induced current (EBIC) measurements were used to determine the position of the p-n junction. On several wafers, an SEM was used to determine cap and active layer thicknesses on the individual laser diodes after threshold current measurements were completed. Capacitance-voltage, current-voltage, and relative optical power output vs current measurements were performed on some devices.

The capacitance-voltage measurements indicate that samples implanted with the "nondiffused" Be-implant schedule have fairly abrupt junctions, while samples implanted with a "diffused" Be-implant schedule have linearly graded junctions. This is indicated in Fig. II-2 which plots $1/C^2$ and $1/C^3$ vs applied voltage for a "nondiffused" and "diffused" diode. The corresponding effective carrier concentrations vs depletion width are shown in Fig. II-3. These results differ from those in GaAs (Ref. 16) where Be-implanted profiles generally become sharper or more abrupt on diffusion, but are consistent with those previously reported for InP (Ref. 18).

Threshold current densities of both "nondiffused" and "diffused" implanted lasers were comparable to those obtained using conventional Zn doping. The relative power output vs current of a typical laser is shown in Fig. II-4. This particular diode had a threshold current density of 2.2 kA/cm^2 and was from a wafer implanted at 150°C with the "nondiffused" Be-implant schedule. It has a cap thickness of 1.5 μm and an active region

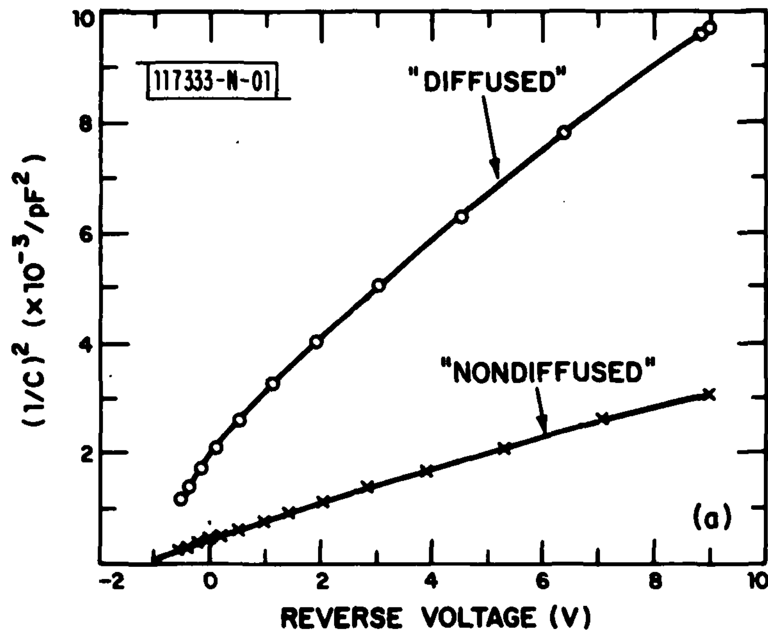

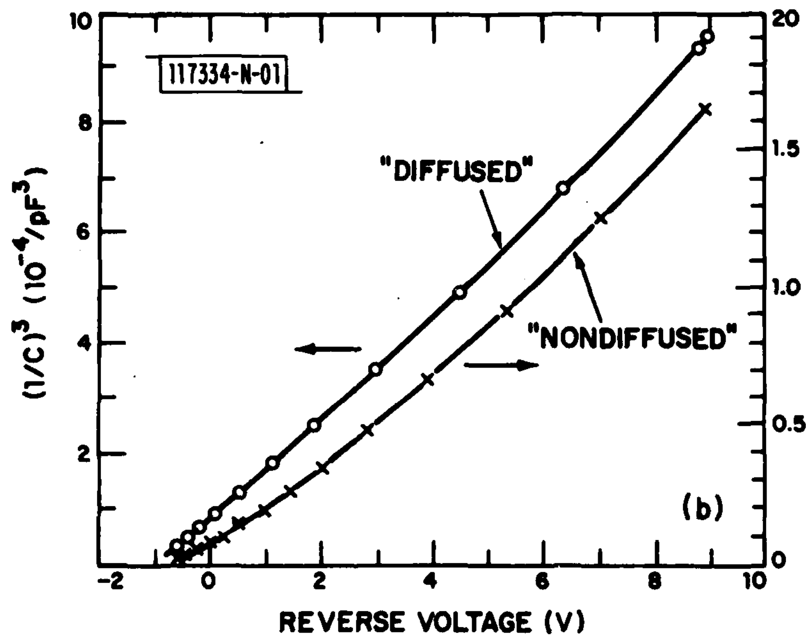

Fig. II-2. Capacitance-voltage properties of "nondiffused" and "diffused" Be-implanted InP/GaInAsP/InP samples: (a) $1/C^2$ and (b) $1/C^3$ vs applied reverse voltage.

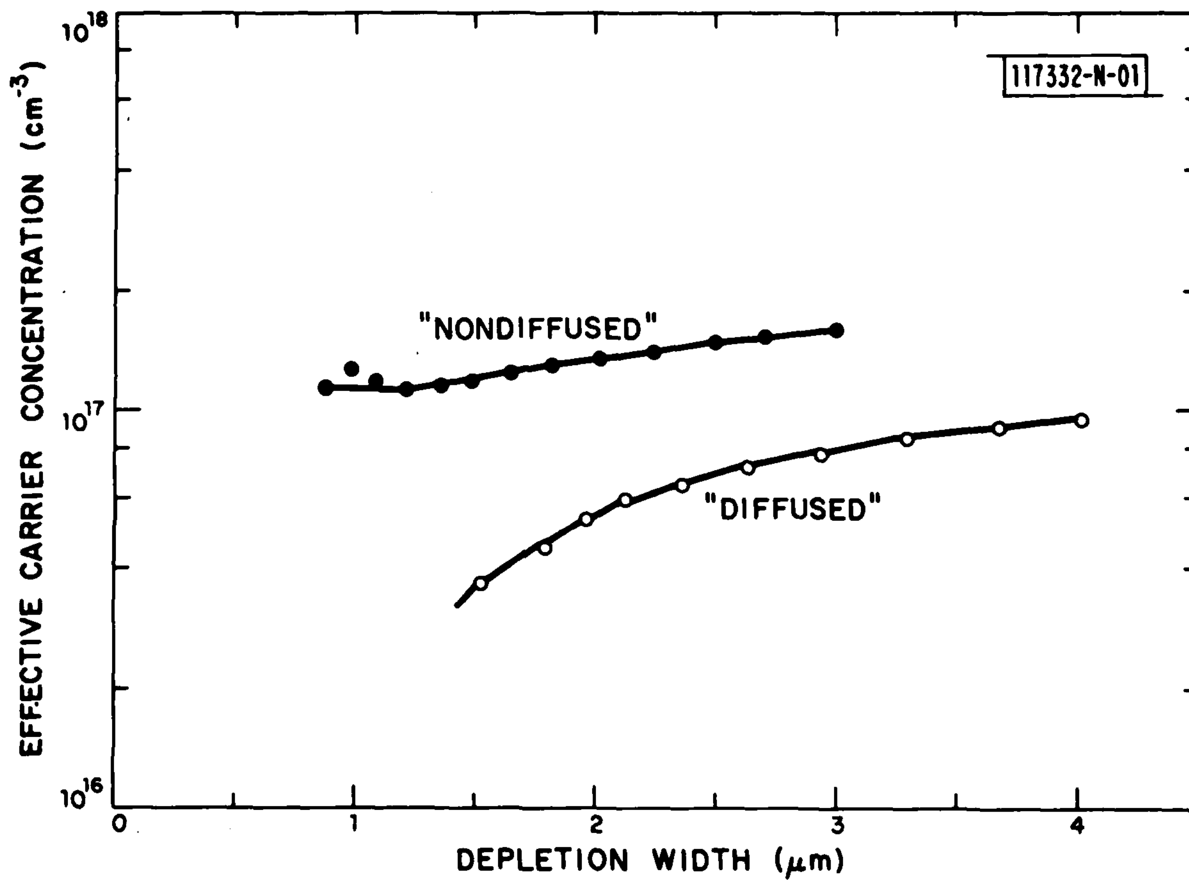

Fig. II-3. Effective carrier concentration vs depletion layer width derived from capacitance-voltage measurements on "nondiffused" and "diffused" Be-implanted InP/GaInAsP/InP samples.

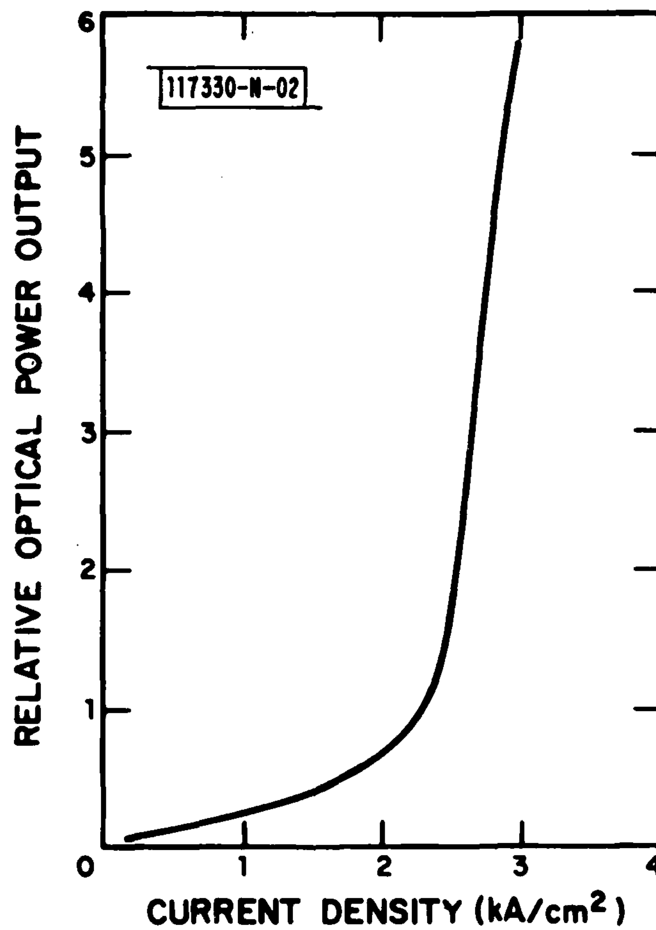

Fig. II-4. Relative power output vs current for a typical broad-area "nondiffused" Be-implanted GaInAsP/InP laser diode.

thickness of 0.3 μm. The threshold current densities of lasers from several wafers are plotted in Fig. II-5 as a function of active layer thickness. The open symbols represent threshold current densities plotted at the average active layer thickness measured on the wafer from which the laser was made, while the filled-in symbols represent those plotted at the active layer thickness measured on the individual laser diode. The dashed line represents the best (i.e., lower limit) threshold current density vs active layer thickness achieved on lasers grown in the same LPE growth system using conventional Zn doping during the growth of the InP cap layer.[22] The nominal threshold current density ($J_{nom} = J_{th}/d$, where J_{th} is the threshold current density and d is the active layer thickness) obtained from the slope of this line is 4.6 kA/cm^2-μm and is representative of the current state of the art of broad-area lasers in the GaInAsP/InP material system.[22] The lowest threshold current density measured in an implanted laser was 1.2 kA/cm^2, corresponding to a J_{nom} = 4.2 kA/cm^2-μm. A more typical lower value of J_{th} measured on wafers with thin layers (0.25 to 0.35 μm) was 2.0 kA/cm^2. On most wafers, the majority of lasers had a nominal threshold current density within a factor of 2 of 4.6 kA/cm^2-μm. Although lasers implanted with the "nondiffused" Be-implant schedule have had slightly lower nominal threshold densities than those implanted with the "diffused" schedule, the data are not sufficient to permit any definite conclusions at this time.

As mentioned previously, the thickness of the InP cap and the uniformity of this layer are important parameters which must be controlled in order to achieve reproducible results. This is especially true for lasers implanted with the "nondiffused" Be-implant schedule. For a given maximum implant energy, if the cap layer is too thick the implanted p-n junction will be in the top InP, resulting in either high threshold current densities or no lasing at all. Cap layers with nonuniform thicknesses cause variations in the position of the p-n junction, which can result in nonuniform injection and wide variations in threshold current densities. Nonuniform thicknesses are likely the more serious problem since cap layers which are uniform but

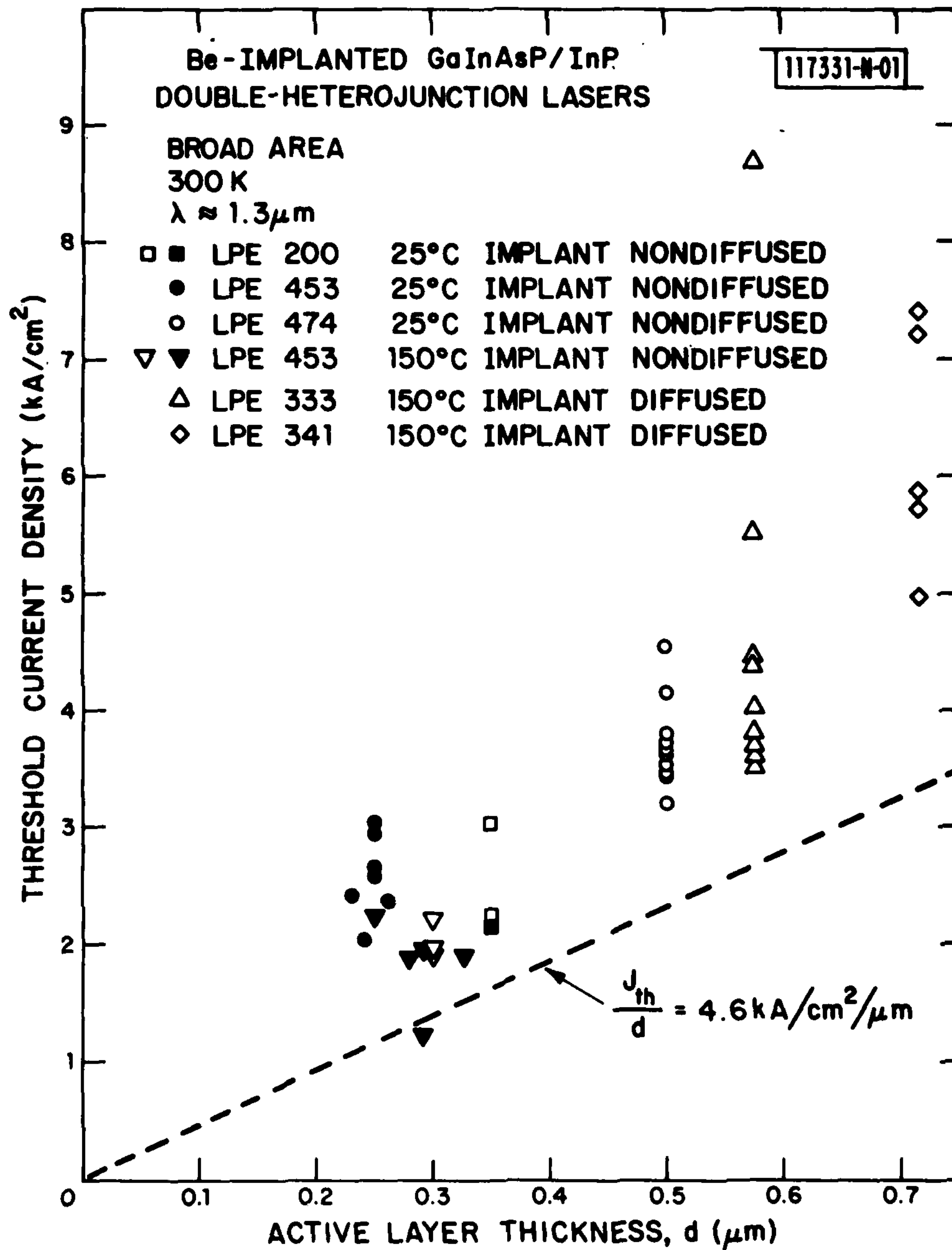

Fig. II-5. Threshold current densities of broad-area Be-implanted GaInAsP/InP double-heterojunction lasers plotted as a function of active layer thicknesses. The dashed line represents the best current threshold densities achieved on lasers grown in the same LPE system using conventional Zn doping during the epitaxial growth.

too thick can be etched to the desired thickness. Since the position of the p-n junction is also determined by the background carrier concentrations in the cap, variations in this parameter can have the same effects.

A SEM micrograph of a diode implanted at room temperature with the "nondiffused" Be-implant schedule is shown in Fig. II-6. Superimposed on the micrograph is the diode's EBIC response, which indicates that the p-n junction of this wafer is actually in the InP, but within 0.3 μm of the heterojunction interface. This laser (taken from wafer LPE 200) had a cap thickness of about 1.9 μm and an active layer thickness of 0.35 μm. Even with the junction in the InP the threshold current density of this laser was 2.3 kA/cm^2. Other samples implanted with the "nondiffused" implant schedule

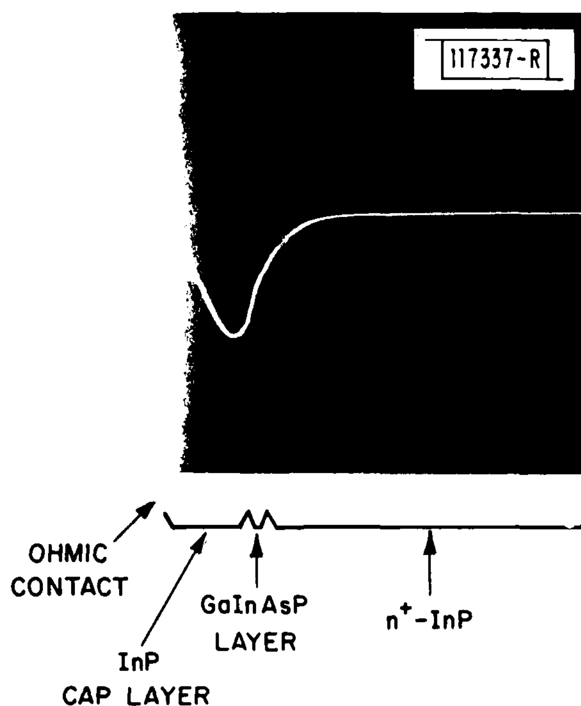

Fig. II-6. An SEM micrograph of a cleaved Be-implanted "nondiffused" GaInAsP/InP laser diode fabricated in a wafer with a 1.9-μm cap layer and a 0.35-μm active layer. Superimposed on the SEM is the EBIC response which shows that the p-n junction lies in the InP cap layer. Even with the p-n junction in the cap layer, this particular laser had a threshold current density of 2.3 kA/cm^2.

had cap thickness of 1.5 to 1.6 μm and junctions nominally at the heterojunction interface. The InP cap thickness, however, cannot be made arbitrarily small. As is well known, a thin cap layer, especially on a wafer which also has a thin active layer, can result in an increased threshold current density because the tails of the guided optical mode penetrate to the p-type ohmic contact. Some increase in threshold current density due to this effect is very likely occurring in the "nondiffused" lasers reported in this section, especially those with active layers <0.35 μm. If the background carrier concentration of the InP cap was reduced to 10^{16} cm^{-3} or less, a cap thickness of about 2.0 μm could be used without any change in implant parameters. Higher energy Be implants would also permit the use of thicker cap layers.

Thicker cap layers can and have been used for the Be-implanted "diffused" lasers. The "diffused" wafers for which data are plotted in Fig. II-5 had cap thicknesses of 2.5 μm (LPE 333) and 3.0 μm (LPE 341). The Be-implant schedule used for sample LPE 333 had a maximum Be energy of 280 keV, while that used for LPE 341 had a maximum energy of 400 keV. The resultant p-n junction on both samples due to diffusion during the anneal were nominally at the heterojunction interface. Even thicker cap layers could probably be used without any change in implant parameters if longer post-implantation diffusion times were used. The "diffused" lasers have the disadvantage that the Be-concentration profile is no longer controlled entirely by the implant schedule and little is known at present of the effect of high Be concentrations on optical loss. As has been previously noted, slightly lower nominal threshold currents have so far been obtained with the "nondiffused" laser diodes.

In conclusion, broad-area Be-implanted GaInAsP/InP laser diodes operating at 1.3 μm have been fabricated and have threshold current densities comparable to those obtained using conventional Zn doping during the epitaxial growth of the InP cap layer. Both a Be-implant schedule which results in minimal diffusion of the implanted Be and one which results in significant diffusion, and therefore junctions much deeper than expected

from LSS range theory, have been investigated. On most wafers, the average nominal threshold current density J_{nom} has been typically 6 to 8 kA/cm^2-μm. The lowest J_{nom} observed was 4.2 kA/cm^2-μm and was measured on a "nondiffused" laser. Some improvement in threshold current density on "nondiffused" lasers with thin active layers (<0.3 μm) should be possible by increasing the maximum usable InP cap layer's thickness. This could be achieved by either decreasing the cap's background carrier concentration or by increasing the maximum implant energy.

J.P. Donnelly
J.N. Walpole
Z.L. Liau

III. INTRACAVITY LOSS MODULATION OF GaInAsP DIODE LASERS

Intracavity loss modulation of diode lasers is a possible alternative to conventional current modulation, particularly in applications requiring large depth of modulation at high rates where current modulation becomes increasingly difficult. Intracavity loss can be produced by integrating an electroabsorption modulator section with a waveguide section and an optical amplifier section as shown in Fig. III-1.

The device structure has been fabricated from a conventional double-heterostructure wafer without the use of a tapered active region thickness or a varying material composition.[23] Optical gain is produced by the forward-biased double-heterostructure amplifier section. The electroabsorption loss takes place in the high-electric-field region of the reverse-biased p-n junction modulator section. The waveguide optically couples but electrically

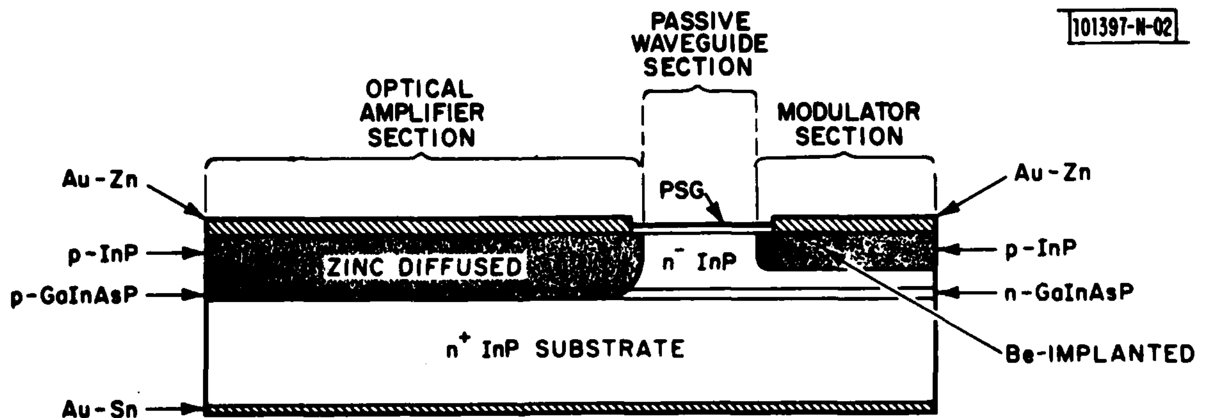

Fig. III-1. Schematic drawing of the laser cross section. The optical amplifier and modulator range in length from 150 to 200 µm and 50 to 75 µm, respectively. The waveguide is 25 µm long. A mesa (not pictured) is etched to provide lateral optical confinement. The endface mirrors are formed by cleaving.

isolates the amplifier and the modulator. Complete isolation is ensured by making the waveguide longer than the sum of the modulator depletion width, the diffusion length of carriers injected from the amplifier section, and the width of any strain-enhanced lateral diffusion of zinc at the phosphosilicate glass-InP interface. The laser mirrors, shown at each end of the structure in Fig. III-1, are formed by cleaving.

The device structure was grown by liquid-phase epitaxy (LPE) on a (100)-oriented InP(Sn) substrate doped to 2×10^{18} cm^{-3}. The step-cooling technique was used to grow a 0.2-μm-thick active layer of $Ga_{0.23}In_{0.77}As_{0.52}P_{0.48}$ and a 2-μm-thick InP cap layer. The net donor concentration in both layers was $\sim 1 \times 10^{16}$ cm^{-3}. An InP buffer layer was not needed because an atmosphere of PH_3 in H_2 was used to prevent thermal etching of the substrate prior to growth.

Zinc was diffused through a window 10 to 12 μm wide in a PSG mask to form a p-n junction for the amplifier section. A modulator section approximately 25 μm wide and 50 μm long was formed by selective implantation of Be ions into the InP cap, followed by annealing at 700°C for 10 min. with a PSG cap layer in a flowing atmosphere of PH_3 and N_2 (Ref. 24). The InP and GaInAsP epitaxial layers were masked and etched to leave a mesa 25 μm wide for lateral optical confinement in the waveguide and modulator sections. Plated Au-Zn contacts were microalloyed to the Zn-diffused and Be-implanted regions through a PSG insulator mask layer, and plated Au-Sn contacts were microalloyed to the n^+ substrate. Ti and Au were sputtered and photolithographically defined to form contact pads on the p side.

Pulsed laser threshold currents of 260 to 300 mA with the modulator open-circuited were typical. Figure III-2 shows the threshold of one device, relative to the threshold with the modulator open-circuited, plotted as a function of the DC modulator reverse bias. The pulsed threshold increased by a factor of about 2.9 upon application of a 20-V reverse bias, just below the modulator breakdown voltage of 22 V.

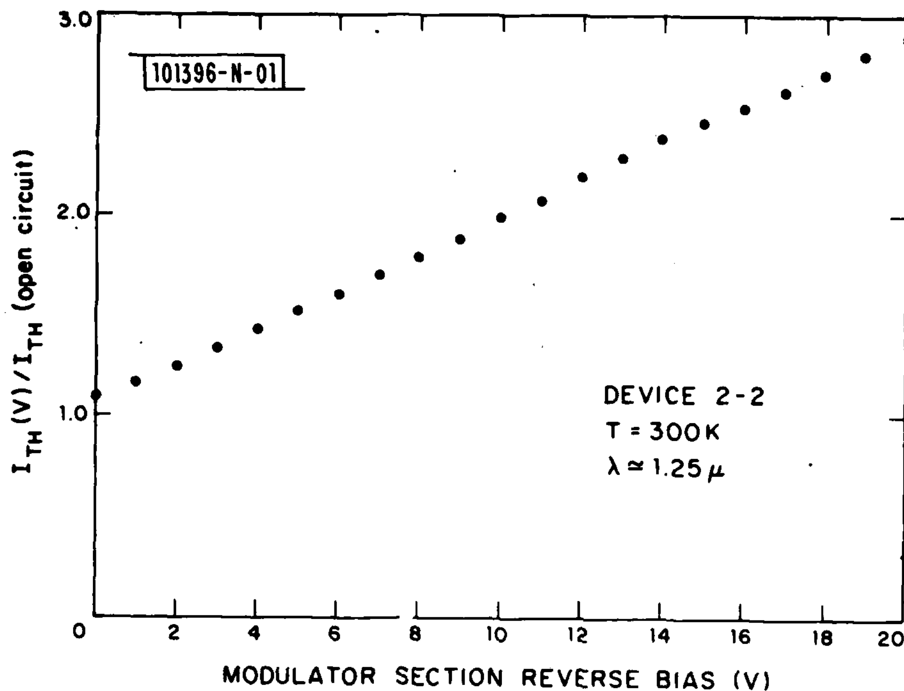

Fig. III-2. Pulsed threshold, normalized to the threshold of the laser with the modulator open-circuited, as a function of the modulator reverse bias.

The lasers have been Q-switched at repetition frequencies between 1.7 and 2.5 GHz by application of a CW microwave signal to the modulator and an electrical pulse to the amplifier. The operating point of the modulator can be determined with a DC bias, which is generally set at a voltage near half breakdown. The electrical pulse to the optical amplifier is then increased until the laser turns on, and the microwave voltage swing is adjusted between the forward-conduction and reverse-breakdown voltages of the modulator. Typically, the microwave drive is about 200 mW into the unmatched circuit. A GaInAsP/InP photodiode with <100-ps rise and fall times is used to detect the laser emission.

The detector output, as displayed on a Tektronix 7104 oscilloscope with 1-GHz bandwidth, is shown in Fig. III-3 for a modulation frequency of 2.2 GHz. It can be seen that the laser responds at this frequency after

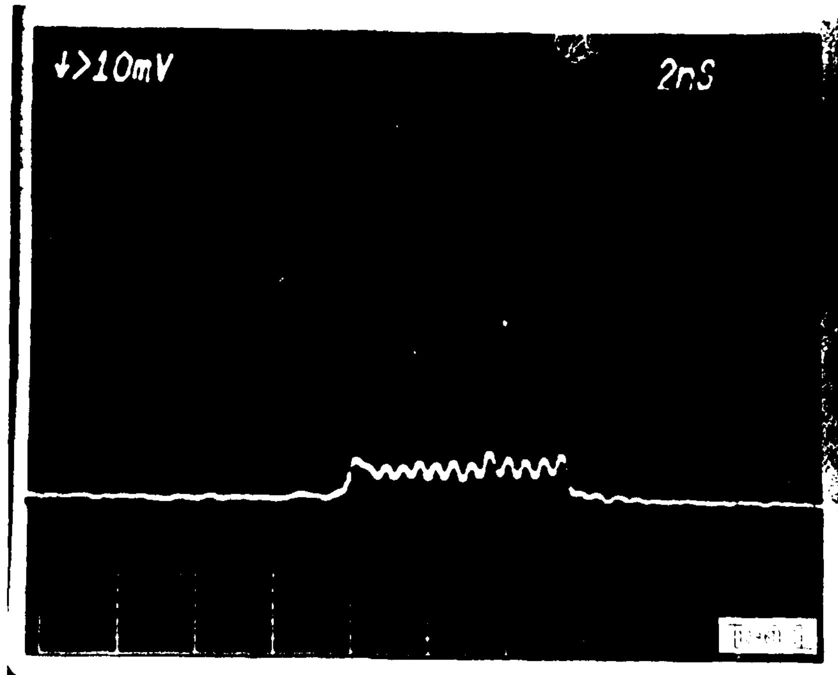

Fig. III-3. Detected waveform of the laser output with a 2.2-GHz modulation signal applied to the modulator. The horizontal scale is 2 ns/major division.

initial transients have decayed. The apparent depth of modulation is limited to about 50 percent by the oscilloscope frequency response, which is down approximately 15 dB at 2.2 GHz. Large-signal modulation has been observed between 1.7 and 2.5 GHz. Above 2.5, the oscilloscope was not capable of providing useful data.

Additional high-frequency measurements, utilizing a sampling oscilloscope, provided a better indication of the depth of modulation. Since the optical-amplifier pulse and the microwave signal are not synchronized, the nonrepetitive nature of the signal precludes a true representation of the waveform. Nevertheless, the observation that the sample points fill in between the baseline of the trace and the highest points indicates that the depth of modulation is substantially greater than

the 50 percent seen in Fig. III-3 and that the laser is likely turning on and off at frequencies as high as 2.5 GHz, the limit of the present measurements.

Further work will be necessary to define the capabilities and limitations of this modulation technique.

D.Z. Tsang J.J. Hsieh
J.N. Walpole J.P. Donnelly
S.H. Groves

IV. MONOLITHIC INTEGRATION OF GaInAsP/InP LASERS WITH PASSIVE OPTICAL WAVEGUIDES

Monolithic integration of passive waveguides with double-heterostructure (DH) lasers has the potential for a number of interesting device applications, including lasers with distributed Bragg reflectors or integrated external cavities, intensity or frequency modulators, and mode-locked DH lasers. Previous attempts to achieve this structure with the GaAs/GaAlAs system, however, resulted in high waveguide loss, high laser threshold current density, and difficulties with control of the liquid-phase-epitaxial growth procedures.[25-29] We have developed a new LPE technique to grow $Ga_{x_2}In_{1-x_2}As_{y_2}P_{1-y_2}$/InP DH passive waveguides integrated with and precisely aligned to previously grown $Ga_{x_1}In_{1-x_1}As_{y_1}P_{1-y_1}$/InP DH laser structures. Uniform waveguide layers and good surface morphology have been achieved in the LPE regrowth. Relatively low threshold current densities (2.4 to 3.1 kA/cm^2) were obtained in a preliminary test of broad-area lasers with one integrated passive waveguide section.

The fabrication procedure is illustrated in Fig. IV-1. Oxide stripes of 500-μm width on 1250-μm centers were first fabricated on a previously grown DH laser wafer. The unprotected sections of the InP cap layer were removed by etching in HCl, after which the oxide mask was removed. To dissolve the sections of the $Ga_{x_1}In_{1-x_1}As_{y_1}P_{1-y_1}$ (Q_1) layer exposed by the HCl etch, two different selective etchants have been used in separate experiments: (a) an aqueous solution of $K_3Fe(CN)_6$ and KOH, and (b) a mixture of H_2O, H_2SO_4 and H_2O_2 (10:1:1 in volume). After the removal of the unprotected Q_1 layer, the sample was dipped in 70°C KOH solution and buffered HF, each for 1 min., and was then immediately loaded into an LPE system with prebaked graphite slider and growth solutions. The LPE system was purged with a mixture of PH_3 and purified H_2, while being heated to 670°C. After approximately 60 min., the system was then cooled to the growth temperature (636°C) in a 10-min. interval. The sample was first slid under the quaternary solution for 10 to

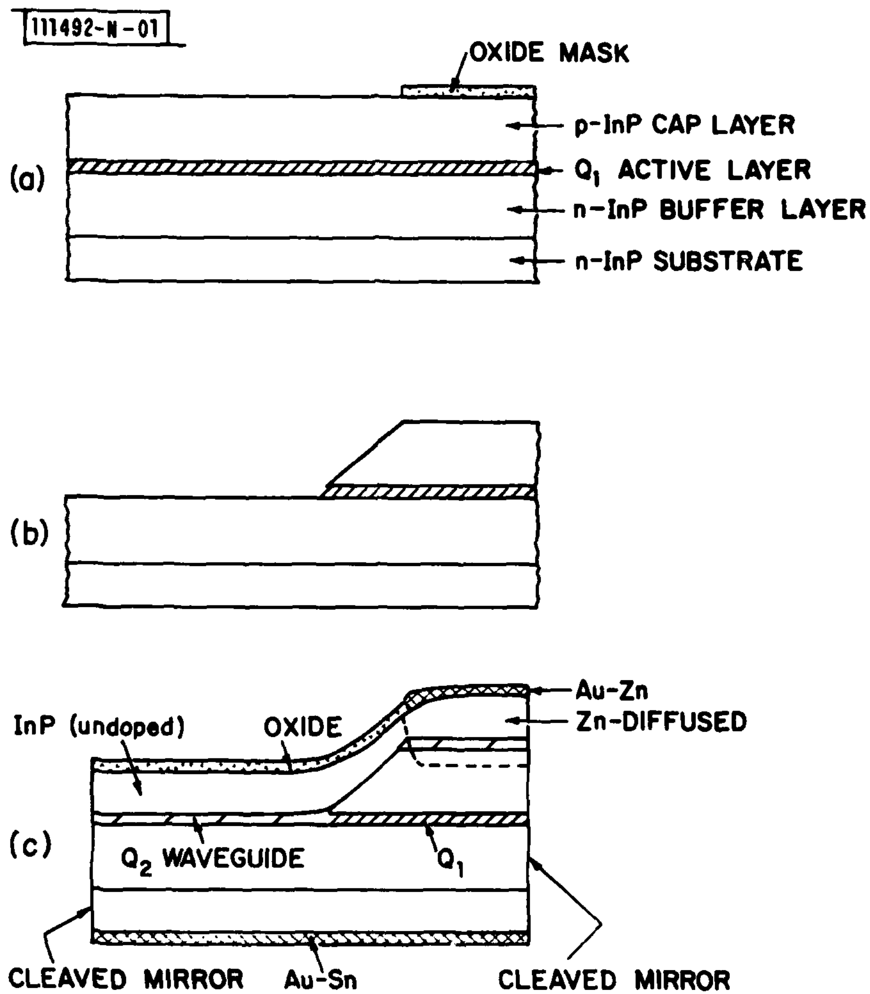

Fig. IV-1. Processing steps for the monolithic integration of a passive waveguide to a GaInAsP/InP DH laser. (a) Double-heterostructure laser wafer, (b) selective chemical etching, and (c) LPE regrowth and device fabrication.

60 s for the growth of the $Ga_{x_2}In_{1-x_2}As_{y_2}P_{1-y_2}$ (Q_2) layer, and then under an InP growth solution for 2 to 10 min. The energy band gap of the Q_2 alloy was 1.03 eV, while that of the Q_1 alloy was 0.95 eV.

Figure IV-2 shows the scanning electron micrographs of the cleaved and stained cross sections of two as-grown samples [(a) and (b)], in which No. 1 and 2 Q-etchants, respectively, were used in the pre-LPE processing. The Q_2 layers show discontinuities at the mesa edges, similar to that observed by Kishino et al. in their fabrication of mesa-substrate buried heterostructure lasers.[30] As evident in Fig. IV-2(a), the Q_2 waveguide layer tended to grow thicker near the waveguide-laser junction. This was found to be related to the shape of the mesa edge formed by the undercutting in the Q_1-layer etching and subsequent vapor-phase migration of InP just before the LPE regrowth. This effect was less pronounced in samples treated by No. 2 Q-etchant which had produced less under-cutting [Fig. IV-2(b)]. Good surface morphologies [Fig. IV-3(a)] have been obtained with high reproducibility for samples treated by No. 1 Q-etchant. In these samples, the Q_2 waveguide layers were generally uniform, smooth and continuous, with very occasional disruptions. However, samples treated by No. 2 Q-etchant contained many discontinuities in the regrown waveguides and good surface morphology has not been achieved [Fig. IV-3(b)].

One sample with all necessary doping concentrations was grown for initial laser testing. In this particular wafer, the Q_2 waveguide layer was fairly thick (1.5 μm near the waveguide-laser junction and 1.0 μm for the rest) compared to the Q_1 active layer (0.3 to 0.4 μm). Broad-area lasers with one integrated passive waveguide section 200 to 350 μm in length and laser section 350 to 440 μm in length showed threshold current densities of 2.4 to 3.1 kA/cm^2, which were ~40 percent higher than those control lasers cleaved from the same wafer but without the integrated waveguides (J_{th} = 1.7 to 2.4 kA/cm^2).

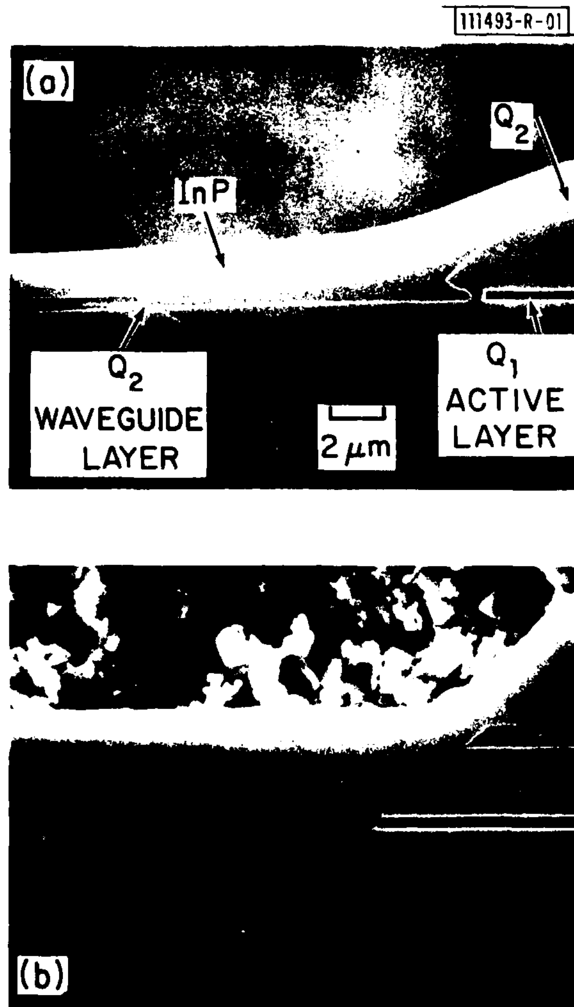

Fig. IV-2. Scanning electron micrographs of the cross sections of two samples in which a DH passive waveguide has been grown integrated with a GaInAsP/InP laser. Different growth features of Q_2 layers were related to different etchants used in the pre-LPE processing.

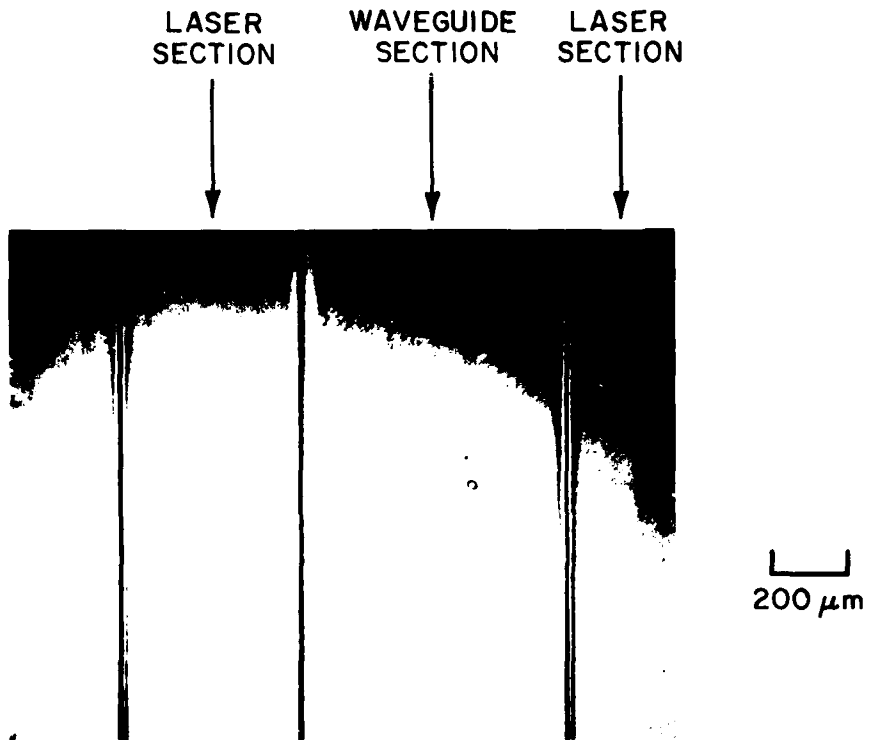

(a)

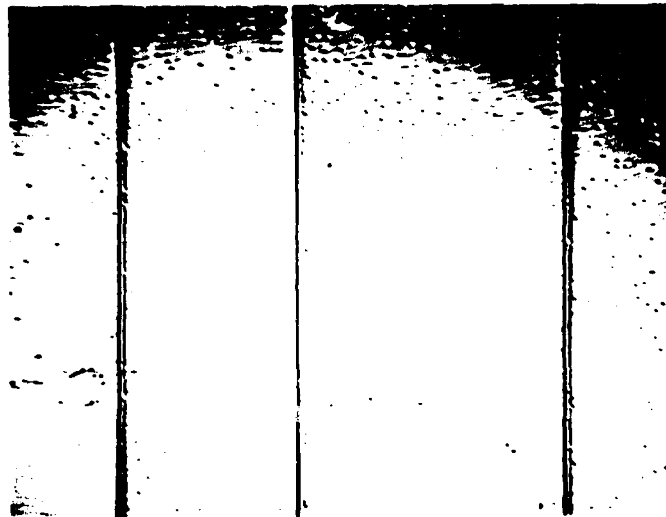

(b)

Fig. IV-3. Nomarski optical micrographs of the surfaces of two different samples after the LPE regrowth of waveguide layers. Difference in surface morphologies was related to different etchants used in the pre-LPE processing.

One possible cause of the somewhat higher threshold current density is the coupling loss due to the mismatch in thickness between the waveguide and the laser active layer. With improved coupling and a thinner laser active layer, lower threshold can likely be achieved. Furthermore, the layer uniformity and good surface morphology achieved in this work should make future fabrication of stripe-geometry devices possible.

Z.L. Liau
J.N. Walpole

V. NOISE CHARACTERISTICS OF InP AVALANCHE PHOTODIODES

Measurements of the excess noise factor as a function of multiplication have been carried out in p^+-n-n^+ inverted-mesa InP avalanche photodiodes (APDs) [see Fig. V-1]. The edge of the mesas were masked[31] to prevent photon absorption in the exposed depletion region and in the p^+-substrate near the junction. This ensures the nearly pure single-carrier injection (holes, in this case) necessary for accurate excess noise factor measurements.

The noise power of the APD as a function of multiplication M was measured at several frequencies and varying levels of illumination by means of a sensitive spectrum analyzer preceded by low-noise transimpedance amplifiers. The excess noise factor F was calculated from the expression $F = I_n^2/2eBI_{po}M^2$ where I_n^2 is the measured mean square noise current added by the light, M is the concurrently measured gain, I_{po} is the primary photocurrent, and B is the bandwidth. The results are shown in Fig. V-2.

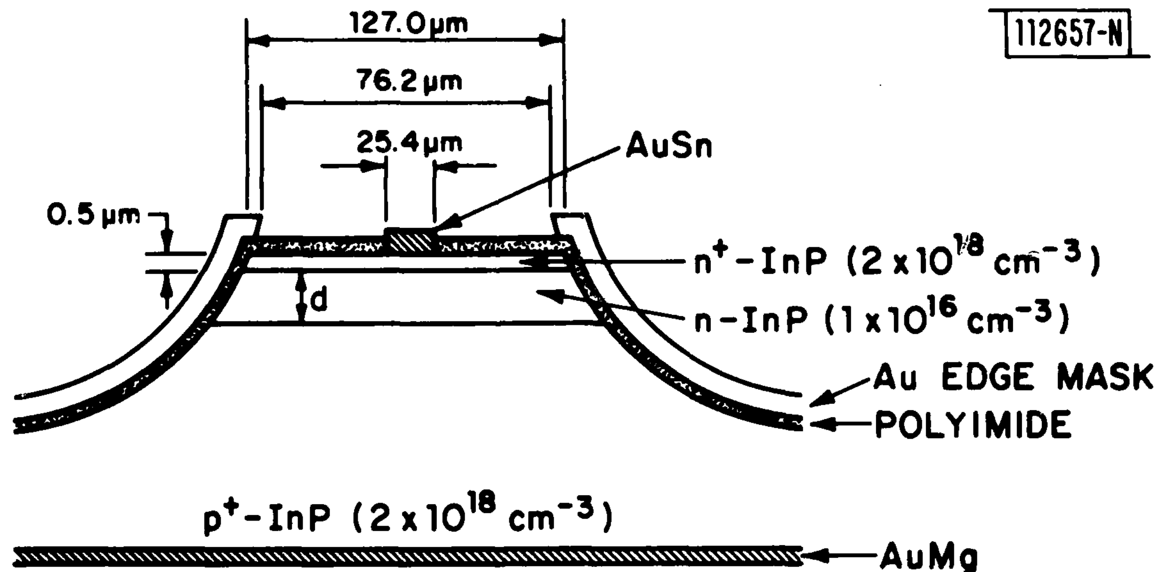

Fig. V-1. InP avalanche photodiode structure and parameters. The n-InP layer thickness, d, was 5 µm and the quantum efficiency 60 percent. An edge mask prevents light incident on mesa sides.

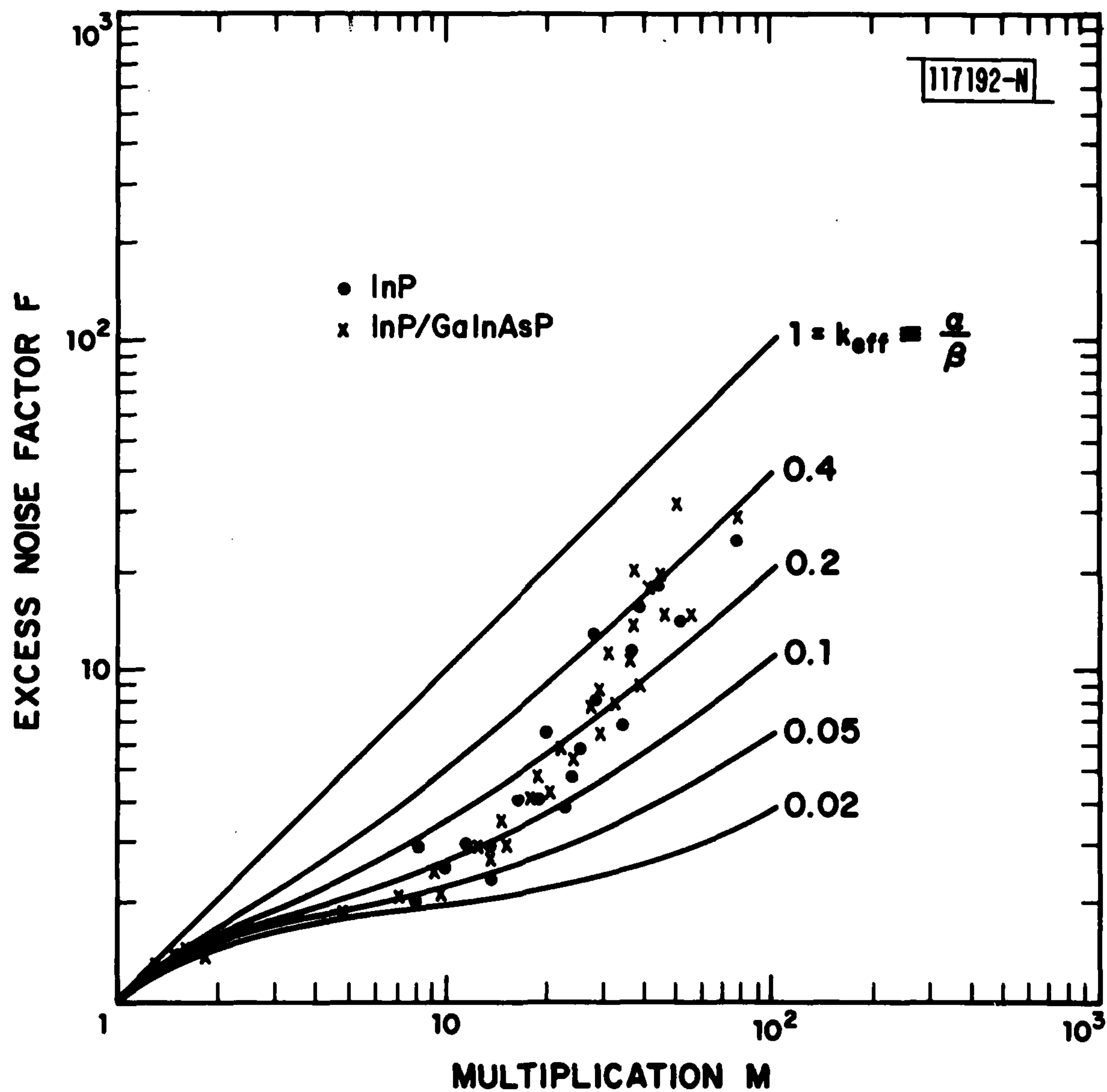

Fig. V-2. Experimental excess noise factor vs multiplication obtained from InP APDs (●) and InP/GaInAsP heterostructure (x) devices described earlier (Refs. 36 and 37). The solid curves are calculated from McIntyre's noise theory (Ref. 32).

The solid curves were calculated from the theoretical expression of McIntyre (Ref. 32): $F(M) = M[1 - (1 - k_{eff}) (1 - M)^2 M^2]$, where k_{eff} is the effective ratio of the field-dependent electron and hole ionization coefficients. It is clear from the figure that the experimental data do not correspond to a single value of k_{eff} over the entire range of multiplication. Low values of F, consistent with a k_{eff} of 0.02 to 0.1, are found for $M \lesssim 10$, but for higher values of M, F increases more rapidly than expected even from the field-dependent McIntyre theory. This result does not agree well with reported noise measurements on diffused-junction devices[33,34] which yield $k_{eff} \sim 0.4$ to 0.6 for $M \lesssim 40$, but is in reasonable agreement with data obtained recently on grown-junction APDs.[35] There is also excellent agreement between the results described here and those obtained previously on GaInAsP/InP heterostructure devices in which the p-n junction is in the InP (Refs. 36 and 37). These results are also shown in Fig. V-2 for comparison. The strong similarity in the magnitude and functional behavior of F(M) for both the simple InP and the composite GaInAsP/InP devices implies that the noise characteristics of the latter are determined by the InP p-n junction rather than the narrow-gap material or the heterojunction interface.

Using a statistical approach, Van Vliet[38] has developed a model to describe avalanche noise which differs from McIntyre's theory in that only a finite number N of possible ionizing events are allowed per pass of a carrier through the depletion region. The excess noise factor determined from this model is shown as the solid curve in Fig. V-3. The discontinuities in the curve correspond to the values of M which have equal probabilities of being achieved with either N or N + 1 ionizations. This represents a piecewise approximation to the continuous behavior that would obtain in reality. The theoretical curve shown in Fig. V-3 represents the best fit to the data of Fig. V-2 and corresponds to a value of k which is approximately 0.2. Theory is in reasonably good agreement with the experimental data for $M \lesssim 10$ but, as in the case of the McIntyre model, the rapid rise in F for the higher values of M is again not predicted.

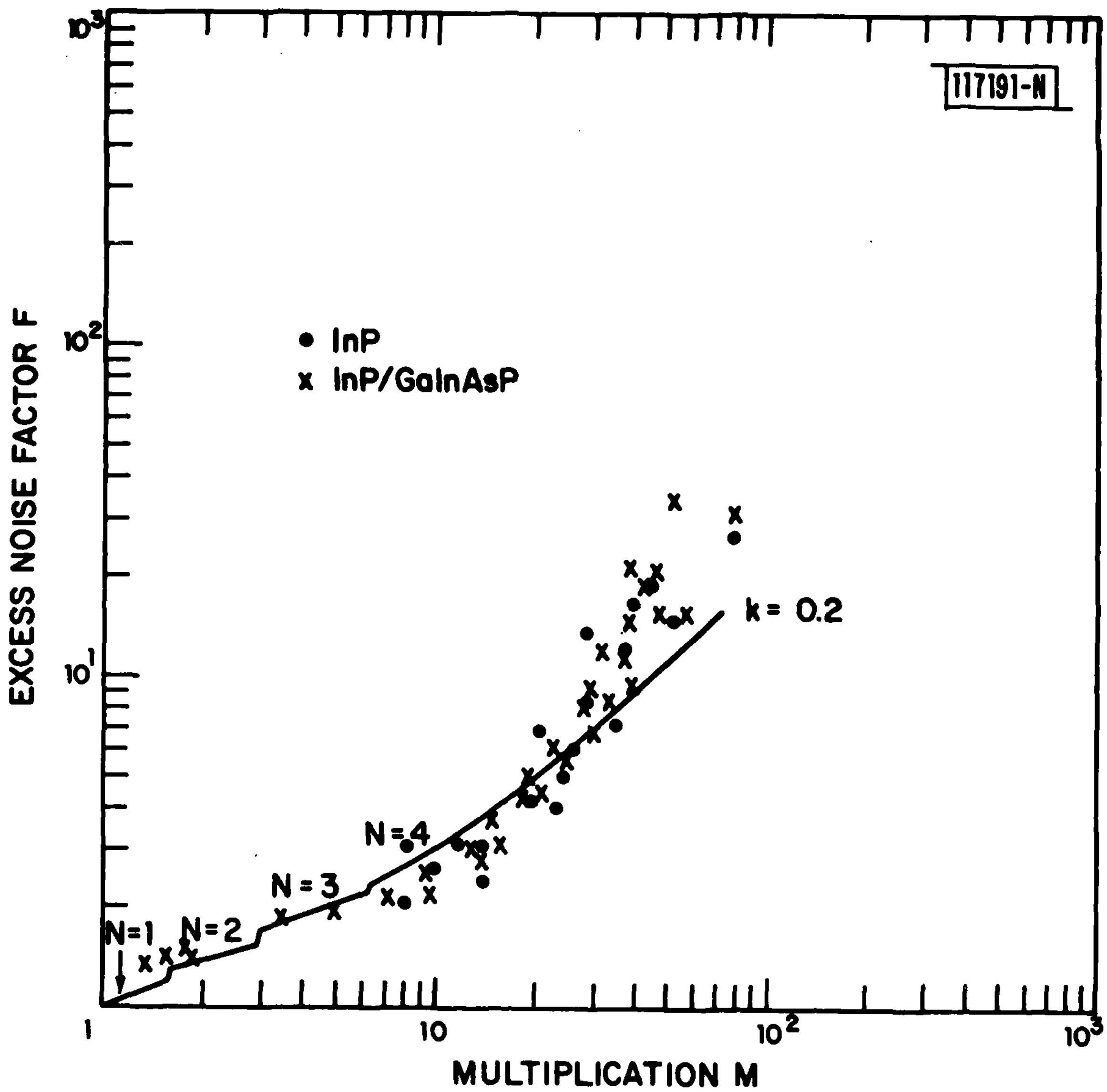

Fig. V-3. Excess noise factor vs multiplication calculated from Van Vliet's noise theory (Ref. 38) for k = 0.2. N is the number of ionizations per carrier pass required to achieve a given value of M. The experimental data are the same as in Fig. V-2.

The fact that the measured excess noise factor F(M) for $M < 10$ agrees reasonably well with McIntyre's theory with $k_{eff} = 0.02$ to 0.1 or Van Vliet's model with $k = 0.2$ makes it clear that the value of the ratio of the ionization coefficients obtained from noise data is very dependent on the model being employed and therefore open to question. In evaluating receiver performance, however, the measured noise power and calculated resulting excess noise factor are the important quantities and these values are desirably low for moderate values of gain in both the Inp and GaInAsP/InP APDs.

V. Diadiuk
S.H. Groves
C.E. Hurwitz

VI. DIFFUSION LENGTH OF HOLES IN n-InP

Hole diffusion lengths of 12 μm in n-InP have been determined by measuring the increase in collection efficiency of an InP photodiode as a function of reverse bias. This diffusion length is much greater than the previously reported value measured on this material by a surface photovoltage technique.[39]

The devices investigated in this study were InP p^+-n-n^+ inverted-mesa structures fabricated using LPE growth and photolithographic techniques.[40] The structure and device parameters are shown in Fig. V-1. The thin (<0.5 μm) n^+ cap layer serves to reduce surface recombination and band-bending effects observed in n-type InP,* but does not significantly reduce the quantum efficiency of the device. For reasons to be discussed below, the thickness d of the n-type InP layer was 5, 16, and 30 μm in the three different wafers tested. The devices were passivated with polyimide[40] and an evaporated Au mask covering the mesa sides was applied to the finished devices. This mask prevented any light from being incident on the exposed depletion region at the mesa sides, thus insuring that the measured photocurrent is due only to the holes that have diffused to the depletion region after photogeneration near the top surface.

By fitting both the magnitude and functional form of the low-bias region of the AC photocurrent vs voltage characteristics, $I_p(V)$, to the current predicted by a model including diffusion and surface recombination, it is possible to determine the diffusion length L_p and surface recombination velocity $\underline{s}$. The theory takes into account the increase in collection efficiency due to the widening of the depletion region with increasing reverse bias but does not include avalanche multiplication. Thus it applies

---

*The surface effects observed in n-type InP include a nonlinear dependence of the output photocurrent on the incident laser power, most likely due to a dead space at the surface resulting from trapping or recombination centers. This will be reported in detail later.

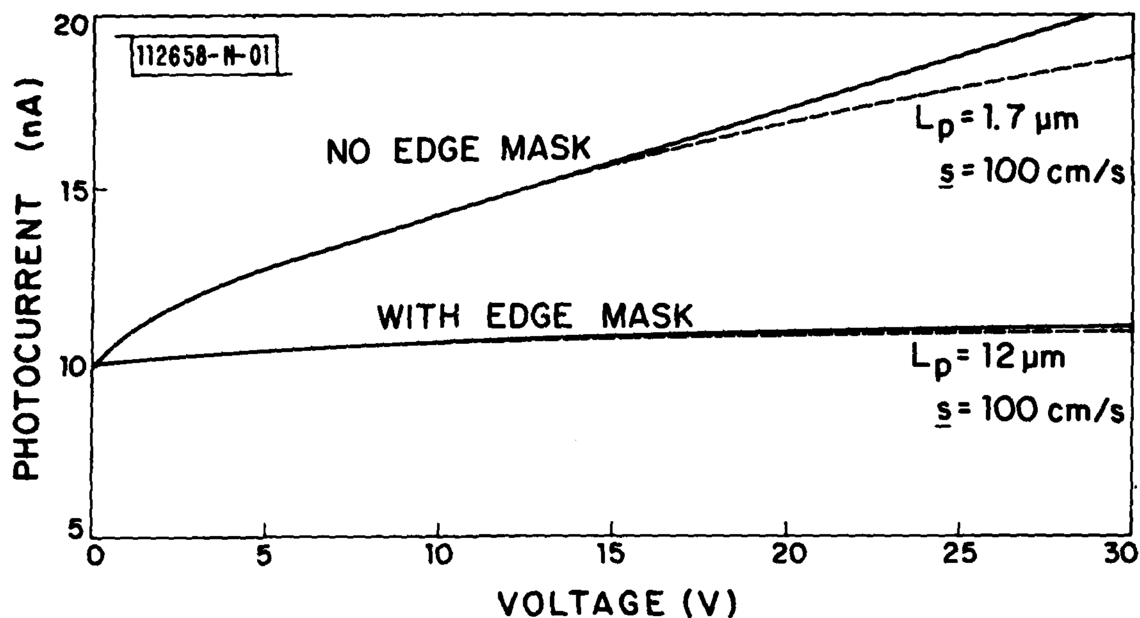

Fig. VI-1. Theoretical and experimental photocurrent $I_p(V)$ as a function of bias voltage with and without edge mask. Values of L_p and s correspond to best theoretical fit to experimental data. Bias at which experimental data depart from theory corresponds to onset of avalanche multiplication.

only to the low-bias portion of $I_p(V)$. Figure VI-1 shows the voltage dependence of the photocurrent measured before and after masking the side of a device, together with the theoretically predicted unmultiplied photocurrent. Without the edge mask, the measured photocurrent rises very rapidly because of direct injection into the increasingly wider depletion region. When this curve is fitted, the result is an artificially low value of L_p, because the entire increase in photocurrent is ascribed to depletion region widening. When the device is properly masked so that the photocurrent is due entirely to light incident from the top, an unambiguous measurement can be made. By fitting the voltage dependence and magnitude of the experimentally measured photocurrent, accurate values of L_p and s can be obtained.

By using samples of three different n-layer thicknesses, it was possible to confirm the accuracy of the technique and reproducibility of the results over a wide range of values of quantum efficiency (11 to 60 percent). Testing diodes with very thick n-type layers is important because only when $d > L_p$ is the voltage dependence of the photocurrent sufficiently strong to give a sensitive measure of L_p. Using this technique, a consistent set of parameters yielding $L_p \sim 12$ μm and $\underline{s} \sim 100$ cm/s was obtained for samples with $d \approx 0.4\ L_p$, $d \approx 1.3\ L_p$, $d \approx 2.5\ L_p$.

This value of $\underline{s}$ is in agreement with that obtained from photoluminescence.[41] However, the value of L_p obtained from the fitting procedure is in disagreement with both the published photovoltage data[39] and the value of 1 to 2 μm determined by EBIC measurements carried out on the same devices. (Our EBIC data are in agreement with published EBIC results.[42]) The likely reason for this discrepancy with respect to the surface photovoltage data is that those measurements are carried out on n-type InP (with no n^+ cap layer) and, therefore, can be seriously affected by the surface band-bending effects present in moderately doped InP. In the case of measurements using EBIC, the discrepancy is due to the fact that the EBIC technique is not quantitatively valid unless the e-beam penetration depth is at least several diffusion lengths,[43] so that carrier recombination at the cleaved surface upon which the electrons are incident can be neglected. The interpretation of the EBIC data is further complicated unless the distance of the junction from the n^+ surface is also several diffusion lengths. Clearly, neither of these conditions is satisfied here. On the other hand, the photocurrent measurements yield the bulk value of L_p, since the n^+ cap layer largely eliminates surface losses, and the holes, generated near the surface, diffuse through the entire n-layer before being collected.

Assuming a hole diffusion constant of 4 cm^2/s, a minority carrier lifetime of ~360 ns can be calculated from the measured diffusion length. To independently verify this value, transient photoconductivity experiments were carried out.* Though not a direct confirmation, since these measurements

---

*In collaboration with S.R.J. Brueck.

were made at high-injection levels, as opposed to the low-injection regime of the photocurrent experiments, the results obtained were consistent with lifetimes on the order of several hundreds of nanoseconds. These results are also in agreement with the values of the carrier lifetime recently obtained from measurements of the modulation frequency response of the spontaneous emission in semiconductor laser structures.[44]

V. Diadiuk S.H. Groves
C.A. Armiento C.E. Hurwitz

REFERENCES

1. R.E. Nahory and M.A. Pollack, Electron. Lett. 14, 727 (1978); R.E. Nahory, M.A. Pollack, and J.C. DeWinter, Electron. Lett. 15, 695 (1979).

2. Y. Itaya, Y. Suematsu, S. Katayama, K. Kishino, and S. Arai, Jap. J. Appl. Phys. 18, 1795 (1979).

3. P.D. Greene and G.D. Henshall, Solid-State Electron. 3, 174 (1979).

4. R.J. Nelson, Appl. Phys. Lett. 35, 654 (1979).

5. N. Tamari and A.A. Ballman, Appl. Phys. Lett. 39, 185 (1981); also, N. Tamari, Appl. Phys. Lett. 39, 792 (1981).

6. Electrooptical Devices Semiannual Technical Summary, Lincoln Laboratory, M.I.T. (31 March 1981), p. 9, DTIC AD-A112890.

7. F. Stern and J.M. Woodall, J. Appl. Phys. 45, 3904 (1974).

8. P. Asbeck, J. Appl. Phys. 48, 820 (1977).

9. Electrooptical Devices Semiannual Technical Summary, Lincoln Laboratory, M.I.T. (30 September 1980), p. 11, DTIC AD-A103542/7.

10. N. Bar-Chaim, M. Lanir, S. Margalit, I. Ury, D. Wilt, M. Yust, and A. Yariv, Appl. Phys. Lett. 36, 233 (1980).

11. D. Wilt, N. Bar-Chaim, S. Margalit, I. Ury, M. Yust, and A. Yariv, IEEE J. Quantum Electron. QE-16, 390 (1980).

12. D.Z. Tsang, J.N. Walpole, S.H. Groves, J.J. Hsieh, and J.P. Donnelly, Appl. Phys. Lett. 38, 120 (1981).

13. M. Yust, N. Bar-Chaim, S.H. Izadpanal, S. Margalit, I. Ury, D. Wilt, and A. Yariv, Appl. Phys. Lett. 35, 795 (1979).

14. J.P. Donnelly, F.J. Leonberger, and C.O. Bozler, Appl. Phys. Lett. 28, 706 (1976).

15. W.V. McLevige, M.J. Helix, K.V. Vaidyanathan, and B.G. Streetman, J. Appl. Phys. 48, 3342 (1977).

16. M.J. Helix, K.V. Vaidyanathan, and B.G. Streetman, IEEE J. Solid State Circuits SC-13, 426 (1978).

17. C.A. Armiento, J.P. Donnelly, and S.H. Groves, Appl. Phys. Lett. 34, 229 (1979).

18. W.T. Devlin, K.T. Ip, D.P. Leta, L.F. Eastman, and G.H. Morrison, in Gallium Arsenide and Related Compounds (1978), edited by C.M. Wolfe (The Institute of Physics, London, 1979), Conf. Series 45, p. 510.

19. W.S. Johnson and J.F. Gibbons, Projected Range Statistics in Semiconductors (Stanford University Bookstore, Stanford, California, 1970); also, J.F. Gibbons, W.S. Johnson, and S.W. Maglorgie, Projected Range Statistics (Halsted Press, New York, 1975).

20. J. Lindhard, M. Scharff, and H. Schiott, K. Dan. Vidensk. Selsk., Mat.-Fys. Medd. 33, 1 (1963).

21. J.P. Donnelly and C.E. Hurwitz, Appl. Phys. Lett. 31, 418 (1977).

22. Z.L. Liau, J.N. Walpole, and G.W. Iseler, this report, Sec. I.

23. F.K. Reinhart and R.A. Logan, Appl. Phys. Lett. 25, 622 (1974).

24. J.P. Donnelly and C.A. Armiento, Appl. Phys. Lett. 34, 96 (1979); also Electrooptical Devices Semiannual Technical Summary, Lincoln Laboratory, M.I.T. (31 March 1978), p. 7, DDC AD-A059062/0.

25. F.K. Reinhart and R.A. Logan, Appl. Phys. Lett. 25, 622 (1974).

26. ____________________, Appl. Phys. Lett. 26, 516 (1975).

27. R.A. Logan and F.K. Reinhart, IEEE J. Quantum Electron. QE-11, 461 (1975).

28. F.K. Reinhart, R.A. Logan, and C.V. Shank, Appl. Phys. Lett. 27, 45 (1975).

29. F.K. Reinhart and R.A. Logan, Appl. Phys. Lett. 27, 532 (1975).

30. K. Kishino, Y. Suematsu, Y. Takahashi, T. Tanbun-Ek, and Y. Itaya, IEEE J. Quantum Electron. QE-16, 160 (1980).

31. Section VI of this report.

32. R.J. McIntyre, IEEE Trans. Electron Devices ED-19, 703 (1972).

33. S.R. Forrest, G.F. Williams, O.K. Kim, and R.G. Smith, Electron. Lett. 17, 917 (1981).

34. T. Shirai, F. Osaka, S. Yamasaki, T. Kaneda, and N. Susa, Appl. Phys. Lett. 39, 168 (1981).

35. G.E. Stillman, private communication.

36. Electrooptical Devices Semiannual Technical Summary, Lincoln Laboratory, M.I.T. (30 September 1980), p. 15, DTIC AD-A103542/7.

37. V. Diadiuk, S.H. Groves, C.E. Hurwitz, and G.W. Iseler, IEEE J. Quantum Electron. QE-17, 260 (1981).

38. K.M. Van Vliet, A. Friedmann, and L.M. Rucker, IEEE Trans. Electron Devices ED-26, 752 (1979).

39. S. Li, Appl. Phys. Lett. 29, 126 (1976).

40. V. Diadiuk, C.A. Armiento, S.H. Groves, and C.E. Hurwitz, IEEE Electron Devices Lett. EDL-1, 177 (1980); also, Electrooptical Devices Semiannual Technical Summary, Lincoln Laboratory, M.I.T. (31 March 1980), p. 5, DTIC AD-A092699/8.

41. H.C. Casey and E. Buehler, Appl. Phys. Lett. 30, 247 (1977).

42. I. Umebu, A.N.M.M. Choudhury, and P.N. Robson, Appl. Phys. Lett. 36, 302 (1980).

43. J.J. Oakes, I.G. Greenfield, and L.D. Partain, J. Appl. Phys. 48, 2548 (1977).

44. J.N. Walpole, private communication.

UNCLASSIFIED

SECURITY CLASSIFICATION OF THIS PAGE (When Data Entered)

REPORT DOCUMENTATION PAGE		READ INSTRUCTIONS BEFORE COMPLETING FORM
1. REPORT NUMBER ESD-TR-81-380	2. GOVT ACCESSION NO. AD-A120 428	3. RECIPIENT'S CATALOG NUMBER
4. TITLE (and Subtitle) Electrooptical Devices		5. TYPE OF REPORT & PERIOD COVERED Semiannual Technical Summary 1 April — 30 September 1981
		6. PERFORMING ORG. REPORT NUMBER
7. AUTHOR(s) Charles E. Hurwitz		8. CONTRACT OR GRANT NUMBER(s) F19628-80-C-0002
9. PERFORMING ORGANIZATION NAME AND ADDRESS Lincoln Laboratory, M.I.T. P.O. Box 73 Lexington, MA 02173-0073		10. PROGRAM ELEMENT, PROJECT, TASK AREA & WORK UNIT NUMBERS Program Element Nos. 62702F and 61102F Project Nos. 2306 and 4600
11. CONTROLLING OFFICE NAME AND ADDRESS Rome Air Development Center Griffiss AFB, NY 13440		12. REPORT DATE 30 September 1981
		13. NUMBER OF PAGES 52
14. MONITORING AGENCY NAME & ADDRESS (if different from Controlling Office) Electronic Systems Division Hanscom AFB, MA 01731		15. SECURITY CLASS. (of this report) Unclassified
		15a. DECLASSIFICATION DOWNGRADING SCHEDULE

16. DISTRIBUTION STATEMENT (of this Report)

Approved for public release; distribution unlimited.

17. DISTRIBUTION STATEMENT (of the abstract entered in Block 20, if different from Report)

18. SUPPLEMENTARY NOTES

None

19. KEY WORDS (Continue on reverse side if necessary and identify by block number)

electrooptical devices	proton bombardment	ion implantation
avalanche photodiodes	double-heterostructure	GaInAsP/InP lasers

20. ABSTRACT (Continue on reverse side if necessary and identify by block number)

This report covers work carried out with the support of the Rome Air Development Center during the period 1 April through 30 September 1981.

GaInAsP/InP lasers with highly uniform and reproducible threshold characteristics have been fabricated by careful control of layer thickness and morphology. Reduced threshold current densities of 4 to 5 kA/cm^2-μm were routinely achieved for a wide range of active layer thicknesses.

18. Abstract (Continued)

Broad-area Be-implanted GaInAsP/InP laser diodes have been fabricated. The best results have been obtained using Be implanted and annealed under conditions which minimize diffusion of the implanted ions. Reduced threshold current densities averaging 6 to 7 kA/cm^2-μm and as low as 4.2 kA/cm^2-μm have been measured and are comparable with those of conventional laser structures. Precise control over the thickness and doping of the InP cap layer is required to achieve reproducible results.

GaInAsP/InP diode lasers have been fabricated with an intracavity electroabsorption modulator. The additional loss produced by operating the modulator near maximum reverse bias increased the laser threshold by a factor of as much as 2.9 relative to the threshold with the modulator open-circuited. Large depth of modulation of the laser output has been achieved at frequencies up to 2.5 GHz, the system measurement limit.

A technique has been developed to monolithically integrate a passive waveguide with a GaInAsP/InP double-heterostructure laser for potential use in fabricating modulators and integrated external cavities. Initial tests of broad-area lasers with 400-μm passive waveguide sections showed threshold current densities of 2.4 to 3.1 kA/cm^2.

The noise properties of InP avalanche photodiodes (APDs) with the n^+-n-p^+ inverted-mesa structure have been characterized. The detectors were found to have essentially the same noise behavior as the GaInAsP/InP 1.3-μm APDs with InP p-n junctions, i.e., an excess noise factor which is very low ($F \sim 3$ at $M = 10$) up to gains of 10 to 20 and which rises rapidly for larger multiplication. The results indicate that the noise characteristics of the GaInAsP/InP devices are determined primarily by those of the InP p-n junctions.

Hole diffusion lengths in n-InP of 12 μm have been determined by measuring the increase in collection efficiency of an InP avalanche photodiode as a function of reverse bias. This diffusion length is nearly an order of magnitude greater than the previously reported values measured by surface photovoltage and electron-beam-induced (EBIC) techniques.